JOURNAL OF GEOPHYSICAL RESEARCH, VOL. 112, D13108, doi:10.1029/2006JD008112, 2007

Incorporating water table dynamics in climate modeling: 2. Formulation, validation, and soil moisture simulation

Gonzalo Miguez-Macho,[1] Ying Fan,[2] Christopher P. Weaver,[3] Robert Walko,[4] and Alan Robock[3]

Received 6 October 2006; revised 22 April 2007; accepted 8 May 2007; published 6 July 2007.

[1] In this second part of the two-part series, we discuss the formulation and implementation of groundwater processes into an existing climate model, by linking a groundwater reservoir and a rivers-lakes reservoir with its land surface scheme. We present the parameterization and validation of these processes with river flow and soil moisture observations. We use the new scheme as a tool to investigate the role of the groundwater reservoir in controlling the spatial and temporal structure of large-scale soil moisture fields. We find that where the water table is shallow, the groundwater reservoir is linked to the soil water reservoir through two-way fluxes. At these locations, the role of the groundwater shifts from being primarily a sink to being primarily a source for the soil, as the season progresses from the wet spring to the dry autumn. Through the two-way fluxes, groundwater exerts a certain degree of control on the root zone soil moisture fields; there is an apparent spatial correlation between the distribution of shallow water table and wet soil. Since the water table reflects long-term climatic and topographic forcing and exhibits strong spatial organization, its link to the soil moisture gives the latter a certain degree of spatial organization as well. The slow changing nature of the water table acts to stabilize the temporal variations in soil water, giving the latter stronger seasonal persistence.

Citation: Miguez-Macho, G., Y. Fan, C. P. Weaver, R. Walko, and A. Robock (2007), Incorporating water table dynamics in climate modeling: 2. Formulation, validation, and soil moisture simulation, *J. Geophys. Res.*, *112*, D13108, doi:10.1029/2006JD008112.

1. Introduction

[2] Soil moisture is a key participant in land-atmosphere interaction and an important determinant of terrestrial climate. In regions where the water table is shallow, soil moisture can be coupled to the water table. As reviewed in detail in part 1 [*Fan et al.*, 2007], the role of water table in climate has been implicitly accounted for in several studies [e.g., *Koster et al.*, 2000; *Decharne et al.*, 2000; *Walko et al.*, 2000; *Chen and Kumar*, 2001; *Seuffert et al.*, 2002; *Gedney and Cox*, 2003; *Yang and Niu*, 2003; *Niu and Yang*, 2003] using the TOPMODEL framework [*Beven and Kirkby*, 1979]. These studies recognize the role of topography in controlling soil water, but the precise mechanisms, i.e., lateral groundwater flow and discharge to streams, are not dynamically represented. The water table has also been explicitly accounted for in several studies aiming to improve the land surface schemes of GCMs [e.g., *Habets et al.*, 1999; *Gusev and Nasonova*, 2002; *Liang et al.*, 2003; *Maxwell and Miller*, 2005; *Yeh and Eltahir*, 2005a, 2005b]. These studies have demonstrated the importance of the groundwater reservoir to the simulated soil moisture and streamflow at grid to watershed scales, using observed atmospheric forcing. Water table dynamics have also been directly coupled with the atmosphere [*Gutowski et al.*, 2002; *York et al.*, 2002] in single column experiments. In this study, we contribute to this larger community effort by first, examining the observed water table dynamics (reported in part 1), second, setting the water table as the lower boundary condition of the soil column, third, explicitly tracking groundwater mass balance and lateral flow, fourth, directly accounting for the dynamic exchange of groundwater with rivers and lakes, and fifth, fully coupling land surface and subsurface hydrology with the atmospheric dynamics in an existing regional climate model. Our focus is a self-consistent modeling framework that will allow us to systematically explore the implication of including deeper storage and long-distance groundwater transport to simulations of soil moisture fields at continental scales and soil water memory at seasonal scales, and the subsequent implication to evapotranspiration, boundary layer dynamics and thermal dynamics, precipitation recycling, and further feedbacks to the land surface and subsurface.

[3] Our findings are reported in three papers. In part 1, we discussed the likely role of the water table in influencing the spatial-temporal characteristics of soil moisture, and exam-

[1]Nonlinear Physics Group, Universidade de Santiago de Compostela, Santiago de Compostela, Spain.
[2]Department of Geological Sciences, Rutgers University, Piscataway, New Jersey, USA.
[3]Department of Environmental Sciences, Rutgers University, New Brunswick, New Jersey, USA.
[4]Department of Civil Engineering, Duke University, Durham, North Carolina, USA.

0148-0227/07/2006JD008112$09.00

ined the observed water table depth in the lower 48 states of the U.S. To synthesize the scattered observations, we used a two-dimensional groundwater model to construct an equilibrium water table as a result of long-term climatic and geologic forcing. The model suggests that the water table depth exhibits spatial organization at watershed, regional and continental scales, which may have implications for the spatial organization of soil moisture at similar scales. The observations suggest that water table depth varies at diurnal, event, seasonal, and interannual scales, which may have implications for soil moisture memory at these scales.

[4] In this paper, part 2, we discuss the formulation and implementation of groundwater processes in an existing climate model, the Regional Atmosphere Modeling System, or RAMS (see http://rams.atmos.colostate.edu/). As shown in Figure 1, RAMS includes a detailed land surface scheme, the Land-Ecosystem-Atmosphere Feedback model (LEAF2), as discussed by *Walko et al.* [2000]. In this work, we expand LEAF2 to include the groundwater reservoir (box 4, Figure 1) and the rivers-lakes reservoir (box 3), forming a new land surface scheme called LEAF2-Hydro, as shown in the blue oval. In this report, we discuss the formulation and validation of LEAF2-Hydro (sections 2 and 3), followed by a simulation of soil moisture fields over North America during the warm season of 1997 for two cases, one with the groundwater, and the other without (section 4). In the simulation, we decouple the atmosphere from the land and use observation-based atmospheric forcing, to isolate the contribution of groundwater to the simulated soil moisture fields from that of the forcing. In a subsequent report, we will apply the fully coupled RAMS-Hydro and discuss the effect of groundwater reservoir, through its influence on soil moisture fields, on evapotranspiration, boundary layer structure, precipitation and further feedbacks on the land surface.

2. Linking Groundwater With Rivers-Lakes

[5] The following equation describes the groundwater mass balance in a model cell,

$$\frac{dS_g}{dt} = \Delta x \Delta y R + \sum_{1}^{8} Q_n - Q_r \tag{1}$$

where S_g [L^3] is groundwater storage in a model column, R [L/T] is net recharge or the flux between the unsaturated soil and the groundwater, Q_n [L^3/T] is lateral flow to/from the nth neighbor, and Q_r [L^3/T] is groundwater-river exchange. This exchange occurs in two modes. The first occurs as groundwater discharge into streams where the water table is higher than the stream. This tends to occur in a humid climate where the water table receives sufficient recharge. Such rivers collect groundwater as they travel down the topographic gradient toward the ocean, and are referred to as gaining streams. Here, the river network provides the most efficient drainage for groundwater. The second mode of exchange occurs where the water table is below the streams, and groundwater receives leakage from the rivers above. This tends to occur in a drier climate where rivers are fed by local surface runoff or upstream inflow. Such rivers diminish as they travel down the topographic gradient, and hence are referred to as losing streams. We represent both modes of exchange.

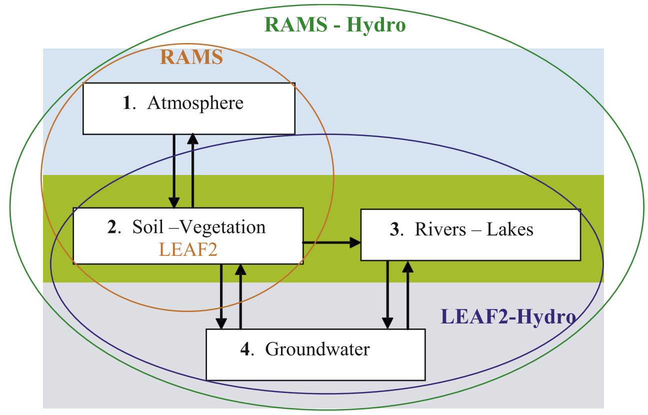

Figure 1. Standard RAMS (orange circle) and its land surface scheme, LEAF2. In this work, we expand LEAF2 to include the groundwater (box 4) and the rivers-lakes (box 3), resulting in LEAF2-Hydro (blue oval). The fully coupled modeling system is called RAMS-Hydro, shown as the green oval.

[6] Consider a gaining stream. Given a river segment, the rate of groundwater inflow depends on three factors: the elevation difference between the water table and the river stage, the hydraulic connection between the two reservoirs (river bed thickness and permeability), and the contact area (length times width of the river segment, neglecting depth). River channels are more or less linear features in the landscape, and even the finest grid spacing in climate models is too coarse for explicit treatment of individual channels. We adopt a statistical approach and make use of total length, mean elevation and width of all streams within a cell. Applying Darcy's law, we have,

$$Q_r = (h - \bar{z}_r)\left(\frac{\overline{K}_{rb}}{\bar{b}_{rb}}\right)\left(\overline{w}_r \sum L_r\right), \qquad \text{for } (h - \bar{z}_r) \geq 0 \tag{2a}$$

where h [L] is the water table elevation in the cell, $\bar{z}_r$ [L] is cell mean river elevation, $\overline{K}_{rb}$ [L/T] is cell mean river bed hydraulic conductivity, $\bar{b}_{rb}$ [L] is cell mean thickness of river bed sediments (often different from aquifer), $\overline{w}_r$ [L] is cell mean river width, and L_r [L] is the length of individual channel segments. The latter two parentheses are often conveniently combined into a parameter called river hydraulic conductance, or river conductance, RC, in groundwater modeling literature, e.g., the widely used USGS model, MODFLOW [*Harbaugh et al.*, 2000]. We can write,

$$RC = \left(\overline{K}_{rb}/\bar{b}_{rb}\right)\left(\overline{w}_r \sum L_r\right) \tag{2b}$$

$$Q_r = RC \cdot (h - \bar{z}_r), \qquad \text{for } (h - \bar{z}_r) \geq 0 \tag{2c}$$

Although RC is physically based and observable, detailed data on river geometry and bed sediments are difficult to obtain for the whole continent. Hence we parameterize RC as discussed below.

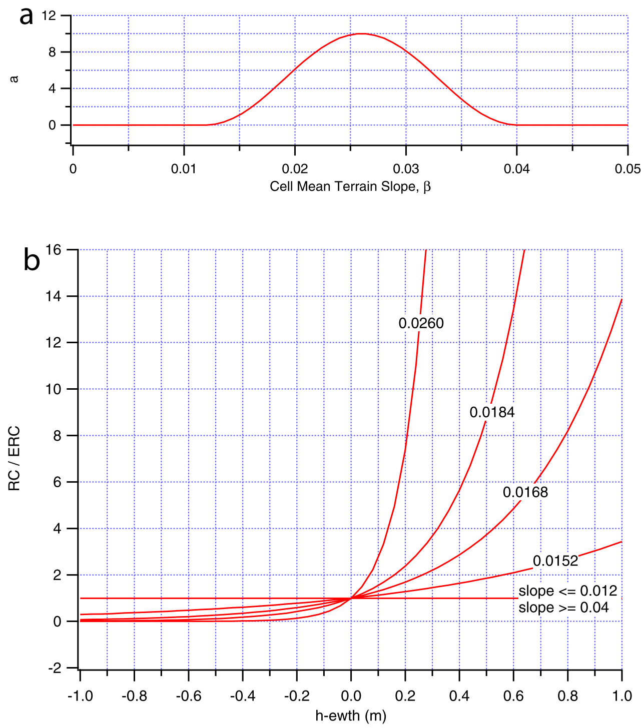

Figure 2. Parameterization of dynamic river conductance, (a) the dependence of parameter a on terrain slope β and (b) the dynamic river conductance (RC/ERC) as a function of water table deviation from equilibrium (h-ewth) at several terrain slopes.

[7] For losing streams, the water table – river difference (first parentheses in equation (2a)) is the same as the distance of flow (denominator in second parentheses, instead of bed thickness of gaining streams), canceling out one another. That is, the hydraulic gradient becomes 1. Thus we have

$$Q_r \equiv \overline{K}_{rb}\left(\overline{w}_r \sum L_r\right) \qquad \text{for } (h - \overline{z}_r) < 0 \tag{2d}$$

We call the right-hand side the "river conductance for losing streams," and treat it as a constant. That is, leakage from the river network to the groundwater is at a constant rate, the only constraint being that it cannot exceed channel storage.

2.1. River Conductance (*RC*)

[8] Although *RC* is physically based and in theory observable, detailed data on river geometry and bed sediment are difficult to obtain for the whole continent. For example, there is no continental database that contains information on stream length and width up to first-order streams. Lacking observations, we estimate *RC* using the inverse method, constrained by river flow observations.

[9] It has long been recognized that river channels expand and contract in response to rainfall events and seasonal hydrologic changes [e.g., *Hewlett and Hibbert*, 1963; *Dunne and Black*, 1970a, 1970b]. During events, a narrow riparian wetland may develop as subsurface stormflow saturates the valleys from below, causing the rivers to widen in effect. River channels may also grow upstream into topographic hollows, causing the rivers to lengthen and branch out. Seasonal change in water table height can switch on and off headwater streams, causing intermittent stream flow. Thus the groundwater-river contact area is a dynamic quantity. These river channel dynamics are elegantly discussed by *de Vries* [1994, 1995] on the basis of observations and theory.

[10] We will treat the parameter *RC* with two parts, an equilibrium part, and a dynamic part. The equilibrium river conductance, or *ERC*, describes the hydraulic connection between the rivers and the groundwater as a result of long-term river channel evolution. It is linked to the equilibrium water table, and represents the equilibrium capacity of the river network in meeting the drainage demand of the land. The equilibrium water table is established in part 1 [*Fan et al.*, 2007]. At equilibrium, the left side of equation (1) vanishes, and discharge to rivers balances recharge and groundwater convergence. By replacing *RC* with *ERC* and *h* with the equilibrium water table head (*ewth*), equations (1) and (2c) give,

$$ERC = \frac{\Delta x \Delta y R + \sum_{1}^{8} Q_n}{(ewth - \overline{z}_r)} \tag{3}$$

where the lateral flow Q_n is calculated using *ewth* from Darcy's Law.

[11] We introduce a parameter called the dynamic river conductance, defined as the product of *ERC* and a function of the deviation of the water table from equilibrium,

$$RC = ERC \bullet \mathrm{F}(h - ewth) \tag{4a}$$

where *F* denotes a function to be determined, which constitutes the dynamic part of the river conductance. Detailed analysis of hydrologic states and fluxes in Illinois suggests that streamflow dependence on water table is nonlinear and concave-up, similar to that of a power law or exponential function [*Eltahir and Yeh*, 1999]. We assume an exponential form for the function F,

$$\frac{RC}{ERC} = \mathrm{F}(h - ewth) = \exp[a(h - ewth)] \tag{4b}$$

The parameter *a* determines how fast *RC* responds to deviations from equilibrium. It is necessarily a function of river valley morphology, for the expansion and contraction of river channels depend on valley profiles [*de Vries*, 1994, 1995; *Marani et al.*, 2001]. In flat terrain, rivers may widen during a wet season or event, but it merely causes a swampy condition where the emergent groundwater is not carried out quickly. In steep terrain, there is little room for channels to grow. Hence the parameter *a* must be a function of local terrain slope within two thresholds. We adopt the sinusoidal curve below,

$$a = amplitude\left\{1 - \cos\left[2\pi\left(\frac{\beta - shift}{wavelength}\right)\right]\right\}, \tag{4c}$$
$$\text{for } 0.012 < \beta < 0.04$$

and $a = 0$ otherwise. It is plotted in Figure 2a for amplitude = 10, shift = 0.012, and wavelength = 0.028. That is, *a* is bounded by terrain slope from 0.012 to 0.04, with a maximum value of 10 at slope of 0.026. These values correspond to relief of 15, 32.5, and 50 m, respectively, between two adjacent cells. They are the result of manual calibration to best reproduce the observed daily streamflow in a 10-year simulation as discussed later.

[12] Figure 2b plots the dynamic river conductance (*RC*/*ERC* = F) in response to water table deviation from equilibrium (*h-ewth*) for several terrain slopes. For example, if the water table rises 10 cm, then at slope = 0.026, corresponding to the maximum *a* in Figure 2a, river conductance will increase by about 3 times, inducing faster drainage. If the water table drops 10 cm, river conductance decreases to 1/3, effectively slowing down drainage. Through this negative feedback, the water table rarely deviates far away from its equilibrium. We found that the water table deviation is on the order of centimeters where the equilibrium water table is deep, to a couple of meters where the equilibrium water table is shallow. This compares well with water table observations discussed by *Fan et al.* [2007], where point observations over a 10-year period and at 21 sites show that deviations from the mean ranged from 10 cm to 5 m. As expected, the observed deviations are larger since they are made at a point, whereas the model gives a 12.5 km grid value.

2.2. River Elevation ($\bar{z}_r$)

[13] The river elevation ($\bar{z}_r$ in equation (2c)), a scale-dependent quantity, requires detailed data on mean river stage for all orders of streams over the continent. Such data are yet to be compiled, and we estimate $\bar{z}_r$ from the equilibrium water table (EWT) obtained in part 1. In obtaining EWT at 1.25 km resolution, river cells appeared naturally because of convergent groundwater flow. These cells function as rivers and the water table elevation at these cells is taken as the river elevation. When no river cells are found within a 12.5 km cell, the minimum land elevation is used. This happens in dry climate where the water table is below local topography and rivers are disconnected with the latter, or in thick and coarse sediments where fast subsurface drainage lowers the water table (e.g., in the High Plains). These elevated rivers convey surface runoff only and occasionally leak into the groundwater, but they do not function as groundwater drainage. Note that the river elevation is not a constant in time; it rises and falls in response to surface runoff, water table change, upstream floods, and downstream tides. For simplicity, we neglect river stage dynamics, since river processes are faster than groundwater and any change in the former is relatively short-lived to affect the latter.

2.3. Rivers-Lakes Mass Balance

[14] We lump all rivers and lakes in a cell into one surface water storage, with a mass balance as,

$$\frac{dS_s}{dt} = Q_h + Q_r + \sum_{1}^{7} Q_i - Q_o \qquad (5)$$

where S_s [L^3] is the surface water storage, Q_h [L^3/T] is hillslope overland runoff given by LEAF2, Q_r is exchange with groundwater, Q_i [L^3/T] is river inflow from the *n*th neighbor, and Q_o [L^3/T] is the river outflow from this cell to the steepest downslope cell. To calculate river flow from an upstream cell to a downstream cell, the last 2 terms in equation (5), we use a linear reservoir model, i.e., the outflow is directly proportional to the storage,

$$Q_o = S_s/k_s \qquad (6)$$

where k_s [T] is a residence time constant, integrating the effect of channel roughness and geometry, channel connectivity, and human regulations. This approach is similar to the variable velocity routing algorithm by *Arora and Boer* [1999] and *Lucas-Picher et al.* [2003].

2.4. A 10-Year Simulation

[15] We apply daily land surface forcing to the coupled groundwater and surface water reservoirs and validate the resulting streamflow with daily observations. Since the groundwater is not linked to the land surface scheme (LEAF2) yet, we prescribe the flux across the land surface using the Variable Infiltration Capacity (VIC) model integration by *Maurer et al.* [2002], as $J = P - ET - Q$, where P is daily precipitation, ET is daily evapotranspiration, and Q is daily surface runoff. This flux J enters a single soil layer, extending from the land surface to the water table. Using the Richard's Equation, equation (7) below, the net flux across the land surface from VIC is translated into a net flux across the water table. This daily flux causes the water table to rise and fall, initiating streamflow response. Such groundwater-generated stream flow, plus VIC surface runoff Q, gives the total contribution to streamflow from each cell.

[16] We simulate this groundwater-surface water linkage for the 10-year period of 1987–1996. Figure 3 plots the simulated and observed daily flow in the Mississippi drainage at five USGS gages, the location of which are given in Figure 4. In general, the simulation agrees well with observed variability at interannual, seasonal (see inset in each time series), and large-event scales. The amount of streamflow is determined by VIC results, which we used to calculate land surface flux to initiate water table and streamflow response. However, the timing of events is affected by our groundwater-river exchange and stream routing. Because we use uniform parameterization for all rivers of the continent (no local tuning), the schemes do not perform equally well in all river basins. We calculate the error in the amount of river flow as daily simulation minus observation, averaged over the 10-year period. The results are given in Figure 3 as "mean error" and Figure 4 in a spatial context as the red number in each basin. The difference between flow at Vicksburg and the sum of the four upstream rivers gives the flow originated in the lower Mississippi valley (lower part of region 07 and upper part of 08). It appears that streamflow is overestimated on the western side of the Mississippi drainage, underestimated on the northern and eastern side, and greatly overestimated in the lower Mississippi valley (below upper Mississippi and above Vicksburg) for its small drainage area. The overestimation in the Arkansas and Missouri basins may be partially caused by groundwater pumping and stream diversion which are in the observed river flow but not accounted for in the model. Groundwater pumping in the High Plains aquifer over the past decades has significantly depleted the groundwater storage and associated streamflow

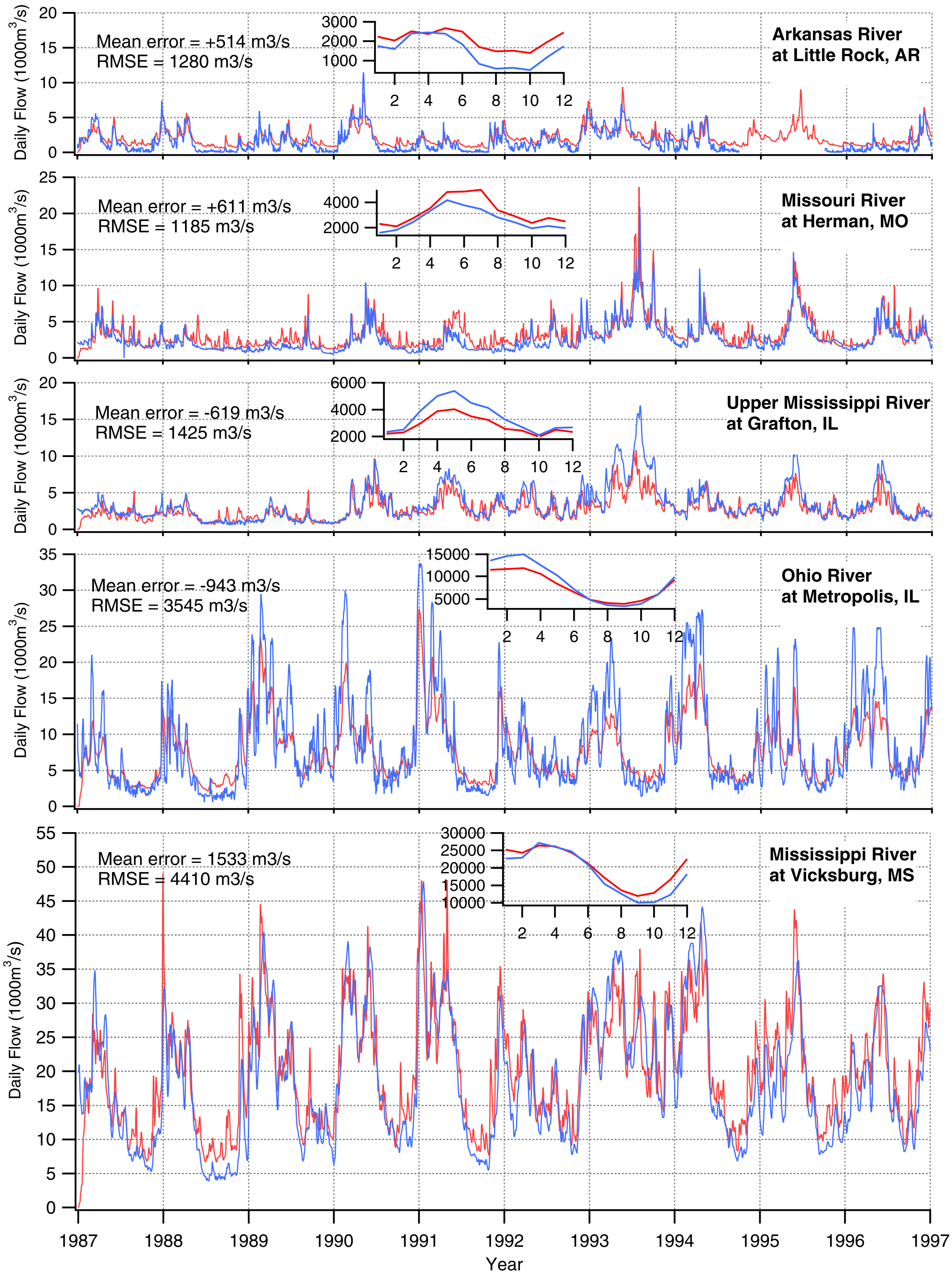

Figure 3. Observed (blue) and simulated (red) daily streamflow (in 1000 m^3/s) at five gauging stations in the Mississippi River drainage, over the 10-year period of 1987–1996. Inset shows the mean seasonal cycle at each site (red indicates model and blue indicates observation).

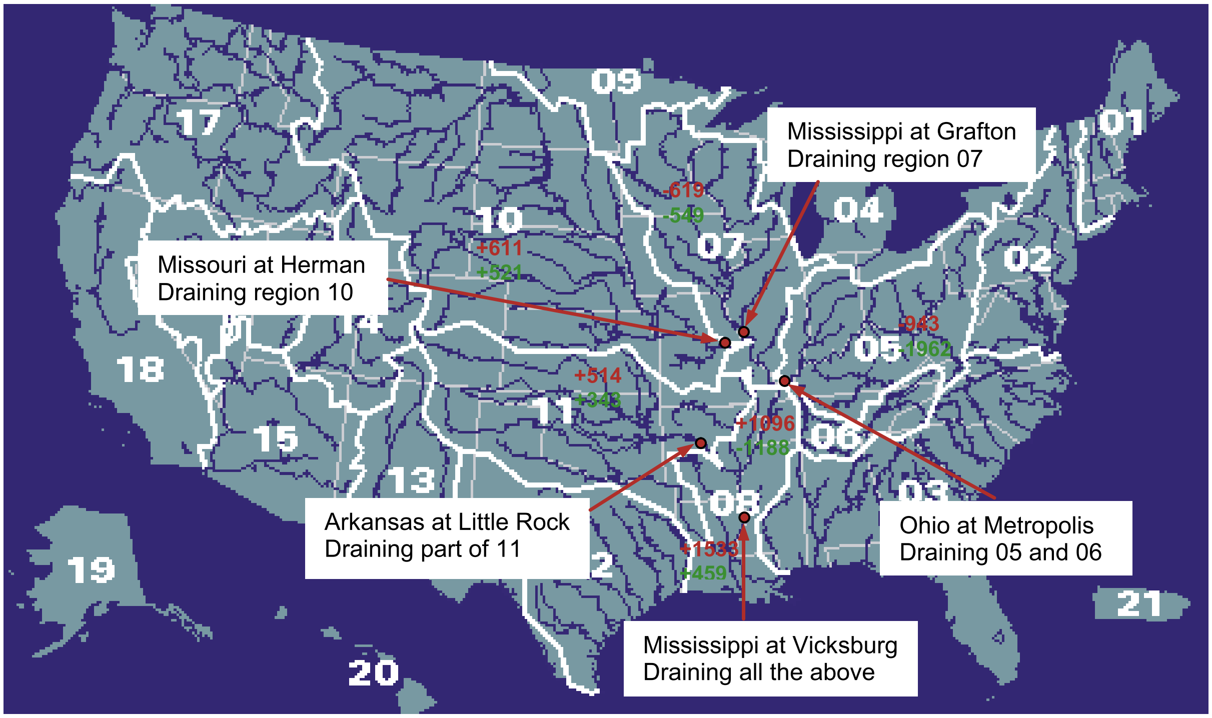

Figure 4. Map of USGS Hydrologic Units (source: http://water.usgs.gov/GIS/huc.html), showing the five stream gauging stations at which daily flow observations are used for validation (Figure 3). The red number in each basin is the 10-year mean model error (in m^3/s), calculated as daily simulation minus observation.

[*Weeks et al.*, 1988], particularly in the dry seasons when irrigation is required.

[17] Since the objective here is to validate the groundwater – surface water link, it would be ideal to compare the simulated streamflow with another model without this link. However, our modeling framework (LEAF2), in its standard version, does not represent streamflow at all, making a direct assessment of the importance of this link difficult. It would also be ideal to be able to separate the contribution of this link from that of streamflow routing through the channel network. However, since we cannot separate the two components in the observations, we cannot evaluate the errors in each with the latter. Thus the discrepancy between the simulated and observed streamflow likely contains errors in both, in addition to not accounting for groundwater withdrawals. We acknowledge these limitations in this stage of our validation.

3. Linking Groundwater With Soil-Vegetation

[18] We link the RAMS land surface scheme, LEAF2 (Figure 1), with the groundwater reservoir by extending the soil column to the water table and using the latter as the bottom boundary condition. The resulting new land surface scheme is called LEAF2-Hydro.

3.1. Water Table as Lower Boundary of Soil

[19] The top part of Figure 5 shows a typical soil layer configuration in LEAF2; a 2.5 m column with 11 layers. Vertical fluxes are up or downward capillary flux (C) and downward gravity drain (G), solved from the Richards' Equation,

$$q = K_\eta\left(\frac{\partial\psi}{\partial z} - 1\right), \qquad K_\eta = K_f\left(\frac{\eta}{\eta_f}\right)^{2b+3}, \qquad \psi = \psi_f\left(\frac{\eta_f}{\eta}\right)^{b} \tag{7}$$

where q is water flux between two adjacent layers, K_η is hydraulic conductivity at given volumetric water content η, ψ is soil capillary potential, b is soil pore size index, and subscript f denotes the quantity at saturation. Values for these soil parameters are obtained from LDAS soil database (http://ldas.gsfc.nasa.gov/) using the relationships given by *Clapp and Hornberger* [1978].

[20] We extend the soil column to the depth of the water table. The new column has 14 layers in the top-4 m (the old layers plus three new 0.5-m-thick layers) and a bottom layer of variable thickness (shaded) that extends to the water table. The choice of 4 m of resolved layers is a balance between the need to resolve the upper most dynamic portion of the column and computation, because it is unfeasible to numerically solve equation (7) over as many layers as needed to accommodate the wide range of water table depths across a continent.

[21] Consider the following two likely water table positions. In scenario 1, the water table is in a layer higher than 4 m depth, shown in Figure 5 as "water table 1." Within this layer, water content in the upper unsaturated portion is obtained by assuming that flux between the layer and the

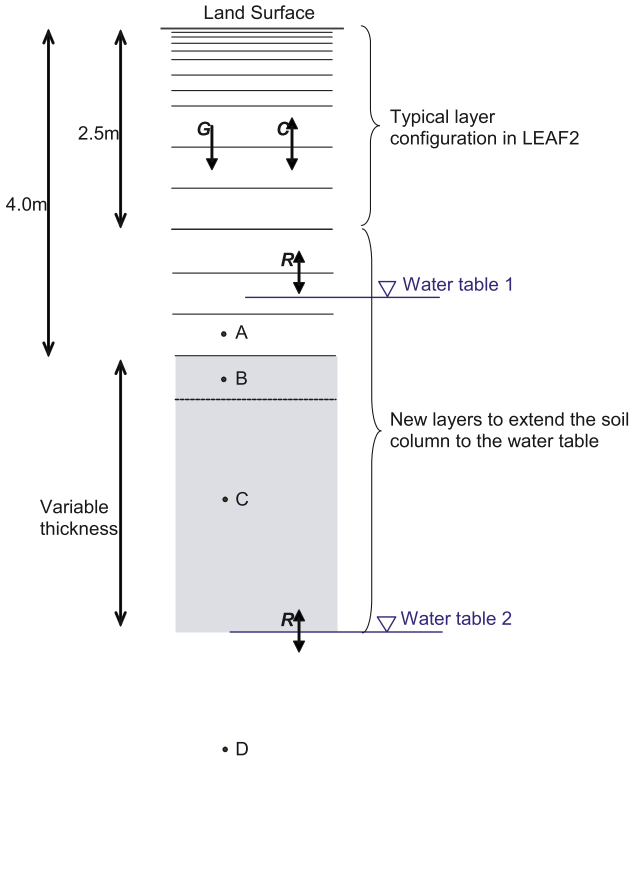

Figure 5. Soil water fluxes in LEAF2-Hydro (G, gravitational drain; C, capillary flux; R, water table recharge) and the extended soil column to the water table.

layer below is zero (no vertical flow between two saturated layers). Setting q to zero in equation (7) leads to,

$$\frac{\partial \psi}{\partial z} = 1, \quad \text{or} \quad \psi_1 - \psi_2 = z_1 - z_2 \tag{8}$$

where subscript 1 refers to the layer containing the water table and 2 the layer below. Using the relationship between ψ and η in equation (7), and with layer 2 saturated, we obtain the water content of layer 1 in the unsaturated portion as,

$$\eta_1 = \eta_{f1} \left(\frac{\psi_{f1}}{\psi_{f2} + z_1 - z_2} \right)^{1/b_1} \tag{9}$$

This water content is used to calculate the layer mean water content by assuming even distribution of total soil water in the layer. The layer mean water content is needed to calculate the flux from/to the layer above, which is taken as water table recharge, R. This flux will cause the water table (wt) to rise or fall, in the amount calculated as,

$$\Delta wt = \frac{R}{\eta_f - \eta_1} \tag{10}$$

Thus the recharge R will fill or drain the pore space between saturation and present water content in the unsaturated part of the layer. The updated water table is then passed to the groundwater routine.

[22] In scenario 2, the initial water table is below 4 m (beyond the resolved depth), shown in Figure 5 as "water table 2." A bottom layer (shaded) is added that extends from 4 m to the water table. The thickness of this layer is variable in space and time. In Figure 5, this layer is centered at point C. Since it can be much thicker than the layer above (problematic for finite difference schemes) an auxiliary layer is added which contains point B (and defined by a dashed line in Figure 5). This auxiliary layer has equal thickness as the layer above which contains point A. The water content of point B is obtained by linear interpolation between A and C. Given water content at A and B, the flux between the two can be calculated. In the same manner, an auxiliary layer is added below the water table, containing point D and with equal thickness as the layer containing C. The gradient between C and D determines the flux between the two, which is the water table recharge R. Knowing the fluxes above and below, water content of the layer with C

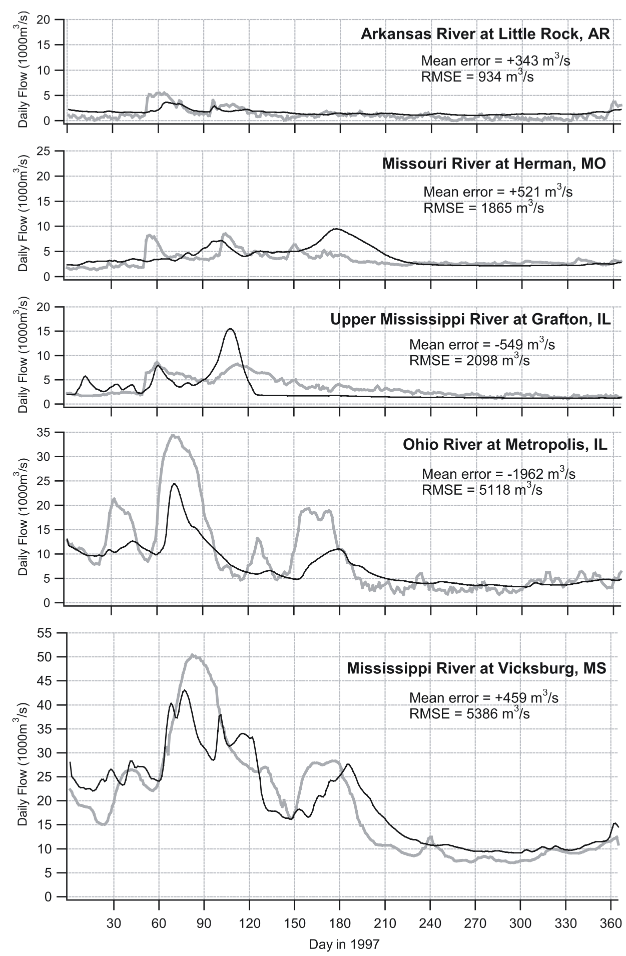

Figure 6. Simulated (black) and observed (gray) daily streamflow at the same five gauging stations (as in Figures 3 and 4) in the Mississippi drainage, from 1 January 1997 to 31 December 1997. The simulation uses LEAF2-Hydro and is forced with observation-based atmospheric variables.

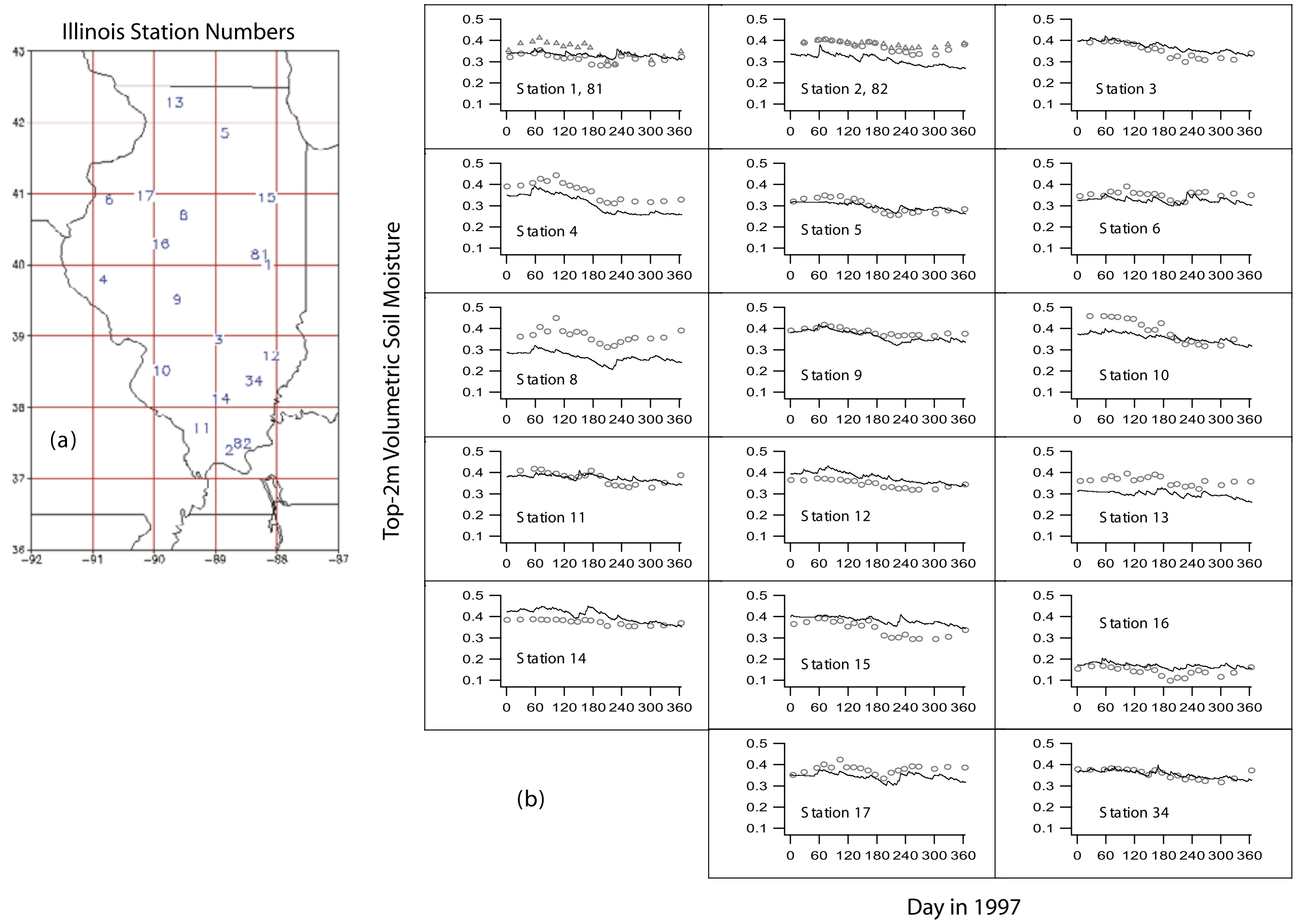

Figure 7. (a) The 19 soil moisture observation stations in Illinois and (b) simulated (black line) versus observed (gray symbols) top-2 m soil water content, 1997. Stations 1 and 81, and 2 and 82, are located in the same model cell, respectively.

can be determined by mass balance as usual. The change in water content is added to or taken away from the water table according to equation (10).

3.2. A 1-Year Simulation

[23] We test and validate the linkage between the soil-vegetation reservoir and the groundwater, which in turn is linked to the rivers-lakes, with a simulation over the year of 1997. The atmospheric forcing is obtained from the VIC archive [*Maurer et al.*, 2002] and National Centers for Environmental Prediction (NCEP)/National Center for Atmospheric Research (NCAR) reanalysis [*Kalnay et al.*, 1996]. Forcing is applied to the land surface at 3-hourly time steps; heat and water fluxes associated with the canopy are integrated every 15 s, heat and water fluxes in the soil every 60 s, water table adjustment every 60 s if within the resolved layers and 0.5 hour if below, groundwater-river exchange and groundwater mass balance adjusted every 0.5 hour, and river flow routing every 5 min (for numerical stability). Comparisons are made with observed daily streamflow at five stream gages in Mississippi and soil moisture observations in Illinois and Oklahoma.

[24] Figure 6 plots the simulated (black) and observed (gray) daily streamflow at the same five gages for 1997. The timing of snowmelt events and ground thawing (affecting infiltration and surface runoff) in the Missouri and Upper Mississippi basins need improvement, which is part of our ongoing effort but beyond the scope of this paper. Overall, LEAF2-Hydro does well with seasonal variations in evapotranspiration and stream flow, and its behavior is similar to that of the 10-year run (Figure 3) forced by VIC land surface fluxes. The mean bias has the same sign in each basin, and the spring-early summer peak flow in the Ohio River is similarly underestimated.

[25] To generate the streamflow volume in Figure 6, we found it necessary to adjust the resistance parameters in LEAF2. All aerodynamic resistance terms were increased. Parameterization of such is a large subject and beyond the scope of the paper. However, linking evaporation with streamflow helped constrain the former with observations of the latter since rainfall reaching the land leaves the land via these two pathways. Streamflow is monitored routinely at many gauges in the world, and these data can be extremely useful for constraining hydrologic partition in climate models.

[26] We validate the simulated soil moisture with observations in Illinois [*Hollinger and Isard*, 1994], archived at the Global Soil Moisture Data Bank [*Robock et al.*, 2000]. Soil moisture at 11 depths (to 1.95 m) is measured at 19 stations (Figure 7a) biweekly in the growing season and

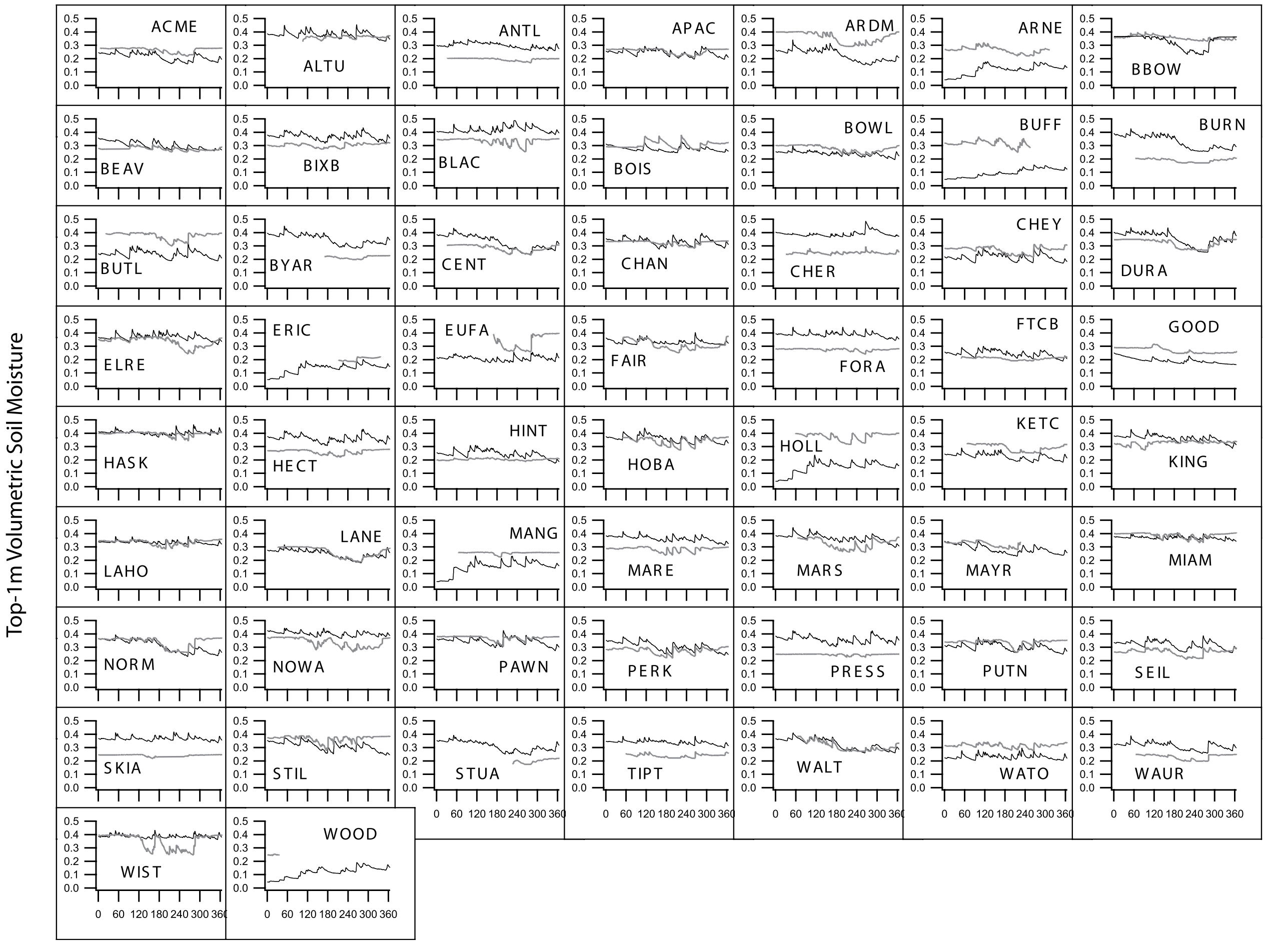

Figure 8. Comparison of simulated (black) and observed (gray) top-1 m soil moisture at the 60 Oklahoma-MESONET stations, 1997.

monthly in winter. Figure 7b plots the simulated top-2 m soil water content versus observations in the cell. The overall comparison is reasonable, given that soil moisture observations were not used for parameter estimation. Where there is large bias, two factors have played a role. The first is the initial soil moisture profile on 1 January 1997, which is at equilibrium with the water table but can be far from the actual distribution. The second is the mismatch of soil texture between a 12.5 km model cell (assigned the most abundant soil type) and an observation point in the field.

[27] We also validate the simulated soil moisture with observations at 60 Oklahoma Mesonet (http://okmesonet.ocs.ou.edu/) sites where soil moisture at 4 depths (to 0.75 m) is observed at 30 min time steps [*Basara and Crawford*, 2000]. Figure 8 plots the simulated (black) and observed (gray) top-1 m soil moisture at 6-hourly time step. At 2 sites, observations are missing at one or more depths for the whole year and comparison at these sites are not shown. There are large biases at some sites; the initial soil water profile plays a role, but the largest cause is the mismatch in soil texture between the model cell and the site [*Robock et al.*, 2003]. Compared to Illinois where the soil is relatively uniform (silty-loam or silty-clay loam, except for Station 16 on a sandy river bank) [*Hollinger and Isard*, 1994], the soils in Oklahoma are much more heterogeneous, ranging from loamy sand to dense clay. The site of ANTL, e.g., reports loamy-sand at all 4 depths, hence the low observed soil moisture. The model cell, however, has sandy-clay-loam for the cell. The clay content in the model but absent at the observation site caused the model soil to hold more water. The site BUFF reports loam, silt, clay, and clay for the 4 depths, but the model cell has loamy-sand throughout, hence the extremely low simulated soil moisture. It seems that the clay content, key to the moisture holding capacity of the soil, cannot be adequately represented in the model using discrete soil types. At site BEAV, where both observation and model cell have the same soil type (loam on top, clay-loam below), the bias due to incorrect initial soil water diminishes as the spin-up continues into the warm season.

[28] We consider the above comparisons reasonable where soil texture is consistent between the model cells and the sites. The comparison, performed in both the humid Illinois and the semiarid Oklahoma, serves as an independent validation that LEAF2-Hydro is capable of simulating the fundamental hydrologic variables in different settings.

4. Effect of Water Table on Simulated Soil Moisture

[29] We now examine the effect of the water table on the simulated soil moisture fields from the above 1-year (1997) simulation. We will focus on the warm season (May through

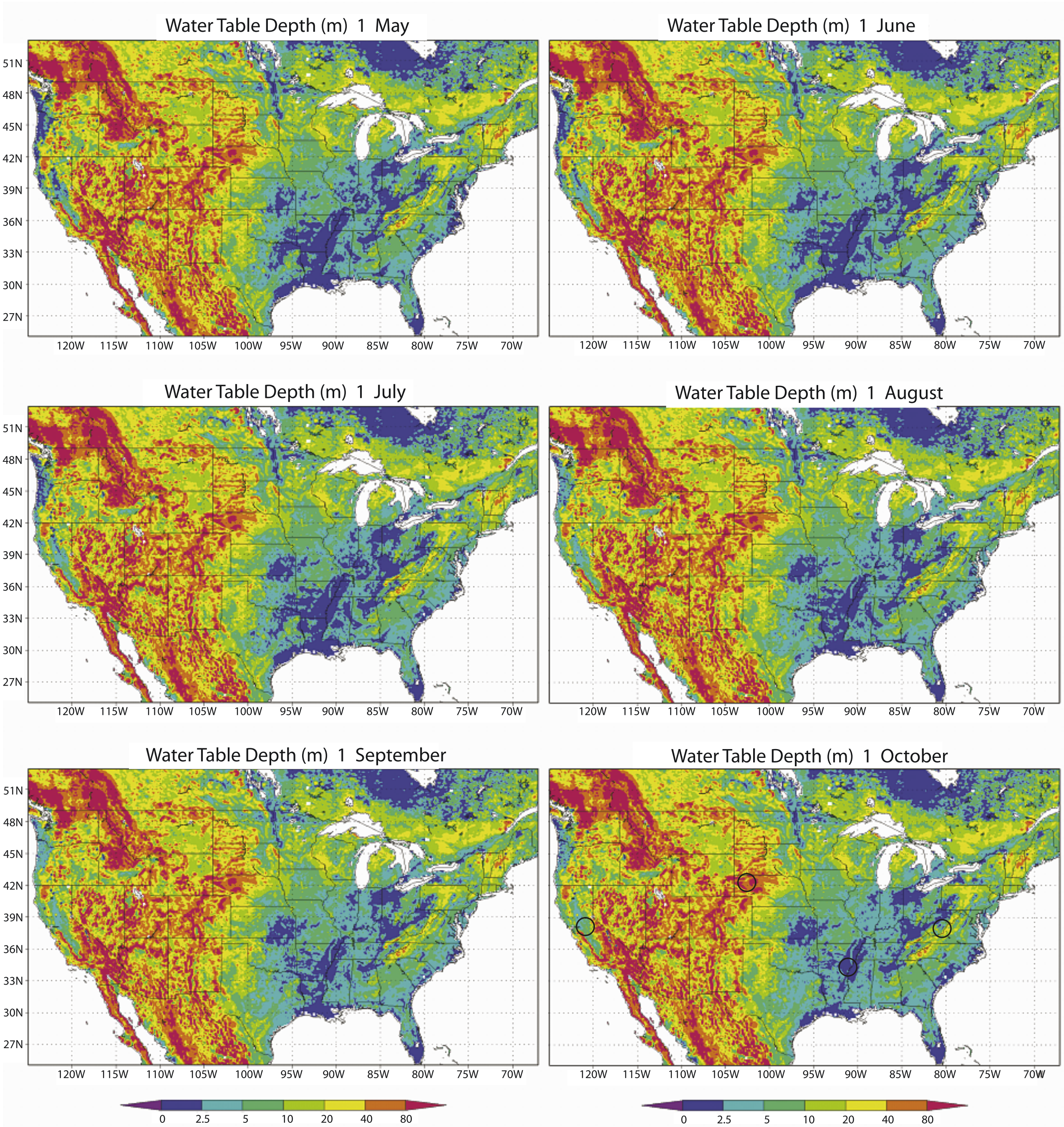

Figure 9. Simulated water table depth (m) on the first day of each month from the WT run. The four small circles on the October map are locations further discussed later.

October) to allow sufficient time for spin-up among the reservoirs (January through April) and to avoid cold season processes where LEAF2-Hydro has difficulties (November and December).

[30] To help isolate the role of the groundwater, we perform another simulation without it, using the commonly adopted free-drain approach, where soil water is allowed to drain out of the land column at a rate set by the hydraulic conductivity at the water content in the bottom layer. The free-drain approach is adopted in most climate models, except in RAMS where there is no soil drainage, which is even more unrealistic and hence not discussed further. The potential drawback of the free-drain approach is that the escaped water is no longer available for subsequent dry-period evapotranspiration. It should work very well where the water table is deep and the soil is sandy, but where the water table is shallow and the soil is clay-rich, it may underestimate the soil water storage and storm water persistence. This may be one of the reasons that recent climate reanalysis must rely on significant soil water nudging where water is added to or removed from the soil column to meet atmospheric demands [e.g., *Roads and Betts*, 2000].

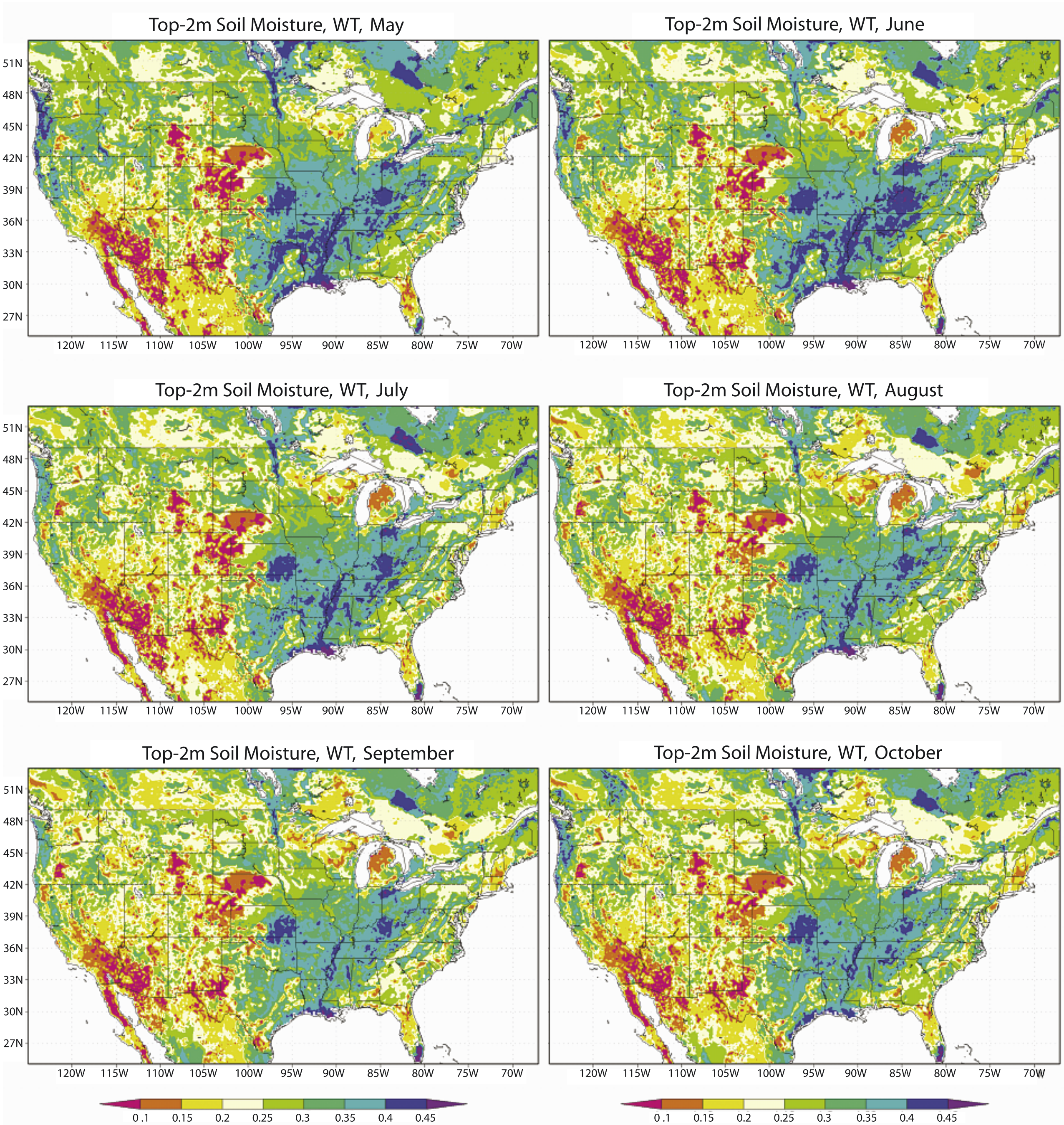

Figure 10. Simulated monthly mean top-2 m soil moisture (% by volume) from the WT run.

[31] In comparing the results from LEAF2-Hydro and free-drain, we will refer to the former as the WT (water table) run, and the latter as the FD (free drain) run.

4.1. Spatial Structure in the Simulated Soil Moisture Fields

[32] We begin by examining the water table depth, given in Figure 9 for each month. A shallow water table (<2.5 m) is found in two types of hydrologic regimes. The first can be found in the humid southeast, where precipitation exceeds potential evaporation. The surplus is removed by surface and groundwater drainage mechanisms. If the drainage is slow, such as in flat terrain, shallow water table results. The second type can be found in the arid and semiarid west, where precipitation is far less than potential evaporation. Here a shallow water table may exist in the topographic lows, not due to a surplus in vertical flux (precipitation-evaporation) as in a humid climate, but due to lateral convergence of river and groundwater flow from the surrounding mountains. Winter precipitation at high elevations gives the region a temporary water surplus that slowly makes its way into the valleys and feeds the water table there. Streams gain their flow from the groundwater in the mountains but lose their flow to the groundwater in the

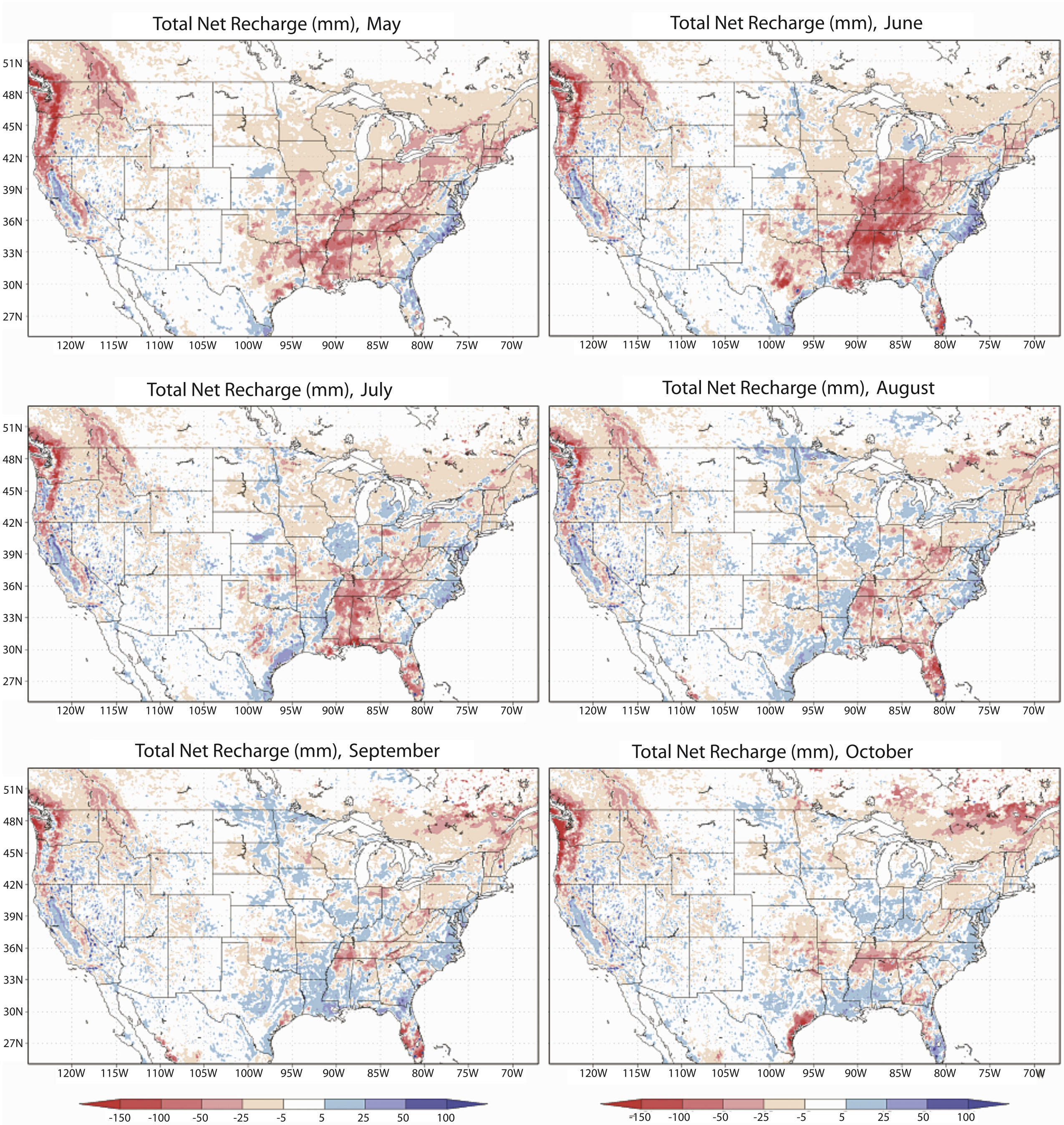

Figure 11. Simulated monthly total flux (mm) across the water table: red indicates downward, and blue indicates upward.

valleys. This lateral redistribution by river and groundwater, and the associated seasonal carryover of water surplus, is a fundamental hydrologic process in such regions. As a result, evapotranspiration in the desert valleys is not as water-limited as it would be in the absence of this lateral transport.

[33] Since the water table exhibits a certain degree of spatial structure, it follows that the soil moisture field, influenced from below by the water table, must to some degree resemble the latter. Figure 10 gives the simulated monthly mean top-2 m (root zone) soil moisture. The resemblance in the spatial patterns between the two sets of maps is apparent. The wettest soil (purple) is found in the lower Hudson Bay drainage, lower Mississippi valley, Mississippi delta and the Florida Everglades throughout the season. These are large perennial wetlands where the soils remain saturated because of abundant vertical surplus and slow drainage. Several large wet patches (dark blue) persist throughout the season, such as in eastern Kansas, in northwestern Ohio, and in north-central Kentucky, all associated with a shallow water table due to shallow bedrock. In addition, in the numerous valleys in the arid and semiarid west and southwest, the valley soils stayed relatively moist

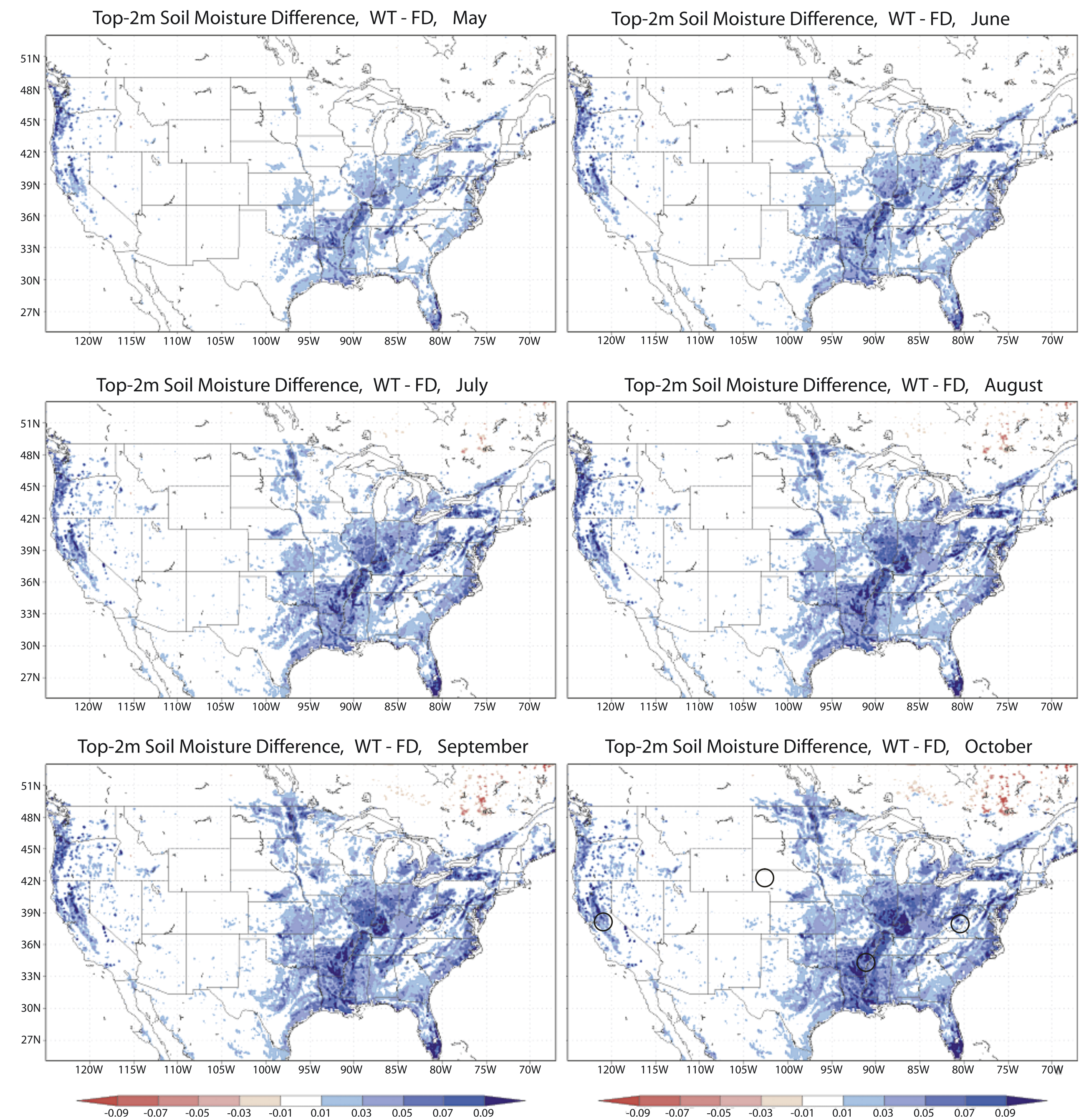

Figure 12. Simulated top-2 m soil moisture difference between WT and FD runs. The four small circles on the October map are locations further discussed later.

in the hottest and driest months. Thus, where the water table is shallow, it exerts a strong control on the spatial structure of the soil moisture field. This control is perhaps just as important in humid regions, and perhaps more important in arid regions, as that due to the precipitation forcing from above.

[34] To further examine the link between the soil-vegetation and the groundwater, we plot in Figure 11 the net flux across the water table for each month, in red for downward flux (water table as a sink) and blue for upward flux (water table as a source). The water table functions both as sink and source for the soil column above; it is a sink when and where large precipitation events occur; the major red patches correspond to heavy rainfall (not shown); it is a source where evapotranspiration exceeds rainfall and water table is shallow. In general, as the season progresses from the wet spring to the dry autumn, its role as a sink weakens and its role as a source strengthens.

[35] The role of the water table can also be assessed by comparing the simulation results with and without it. Figure 12 gives the difference in the simulated top-2 m soil moisture between the WT and FD runs. In the latter, there is no water table, and any surplus soil water drains out freely from the bottom of the 4 m soil column. Since both

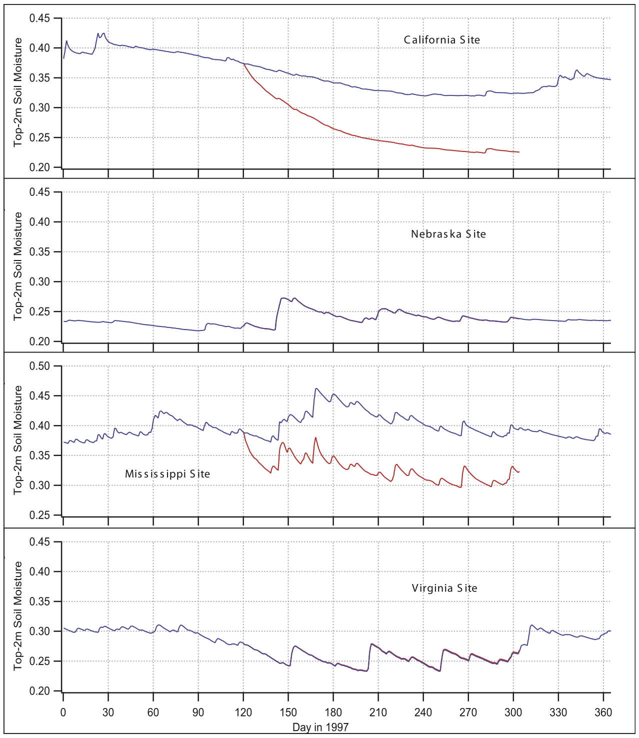

Figure 13. Top-2 m soil moisture time series: blue indicates WT, and red indicates FD.

runs started at identical initial conditions on 1 May, the difference is small in May but grows as the effect of the initial condition diminishes. In the fall, the soils in the WT run are considerably wetter than those in FD over large portions of the continent, but particularly where the water table is shallow. The similarity between Figure 12 and Figure 9 (water table depth) is quite apparent. Over much of the region shown as blue in Figure 12, the water table is deeper than 2 m, therefore the water table does not directly enter the calculation of the top-2 m soil moisture. Yet the slow vertical drainage due to the presence of a water table below, and more importantly, the upward capillary flux from the water table in dry periods, kept the top-2 m soil much wetter than the free-drain scenario. Note that the difference in Figure 12 is likely a conservative estimate due to the fact that they began with identical and water table-induced initial soil conditions.

4.2. Temporal Structure in the Simulated Soil Moisture Fields

[36] Figure 10 also illustrates the direct role of the water table in controlling the temporal persistence of soil wetness, in that a broadly similar soil moisture pattern existed throughout the 6 months. The unsaturated soil is sandwiched between two reservoirs of disparate timescales, and the slow-changing groundwater reservoir below stabilizes its response to the fast-changing atmospheric events above. We note that this persistence at seasonal timescales is not only due to the water holding capacity of the soil, as widely recognized, but also due to the link to the groundwater.

[37] We select four grid cells in the model domain to further examine the time evolution of the soil moisture. The locations are given on the October water table map and soil moisture difference map (Figures 9 and 12). Two sites are from a semiarid climate, one with a deep water table that reflects the vertical, atmosphere-induced water deficit (Nebraska site), and the other with a shallow water table, despite the climate, that is sustained by lateral, topography-induced water surplus (California site). The other two sites are from humid climates, one with a shallow water table that reflects the vertical, atmosphere-induced water surplus (Mississippi site), and the other with a deep water table, despite the climate, because of fast, topography-induced lateral drainage (Virginia site). Thus the four sites represent four distinct end-members in the hydrologic continuum that reflects the interplay between the climate and the geologic forcing.

[38] Figure 13 plots the time series of top-2 m soil moisture at 6-hourly time steps at the four sites, blue from WT, and red from FD, the latter conducted over the 6-month warm season only. The site in California has an annual precipitation $\approx$500 mm and lake evaporation $\approx$1,500 mm, yet the water table is shallow because of lateral transport of winter surplus from the mountains. Since FD does not include lateral transport, it gives a much drier soil. The site in Nebraska is in a semiarid climate, with precipitation of $\approx$500 mm/yr and lake evaporation $\approx$1,000 mm/yr. With no significant lateral input, its deep water table directly reflects the climate, and WT and FD give the same results. The site in Mississippi is in a very humid climate, with annual precipitation $\approx$1,250 mm and lake evaporation $\approx$1,000 mm. Here the shallow water table reflects the climate as well as the slow drainage due to flat terrain. Here FD drains too quickly, resulting in much drier conditions. The site in the steep hills of Virginia, although moderately humid with precipitation $\approx$1,000 mm/yr and lake evaporation $\approx$900 mm/yr, has a deep water table due to fast drainage by groundwater discharge to rivers. Here WT and FD showed little difference. Although we fully recognize the importance of validating the above simulations with observed soil moisture, unfortunately the latter is not available at the four sites, which are chosen to represent four end-members of climate and hydrologic conditions. Thus the above discussion only pertains to the sensitivity of simulated soil moisture to the drainage schemes.

[39] We complete this paper with a synthesis of the temporal behavior of simulated soil moisture in the WT run, in the context of the linked evolution of the soil moisture zone and the groundwater reservoir and their associated fluxes, as shown in Figure 14. The left column plots the relevant time series at the California site, and the right column at the Mississippi site. The diagram in between illustrates the storage reservoirs and the fluxes that link them. For each site, we show daily precipitation, net daily land surface flux (infiltration or evapotranspiration), the soil moisture profile, net daily water table flux, water table depth, and the groundwater-river exchange. At the California site, the wet season is in winter, when the surplus (red flux) reaches the water table and is delivered into local streams. In the dry and warm season, the water table switches its role (blue flux) and supplies moisture to the soil to meet the demands of evapotranspiration. In the absence of lateral flow, this upward flux would significantly lower the water table, but the steady input from subsurface lateral flow keeps the water table relatively shallow. During the period of May to October, capillary loss from the water table to the soil is

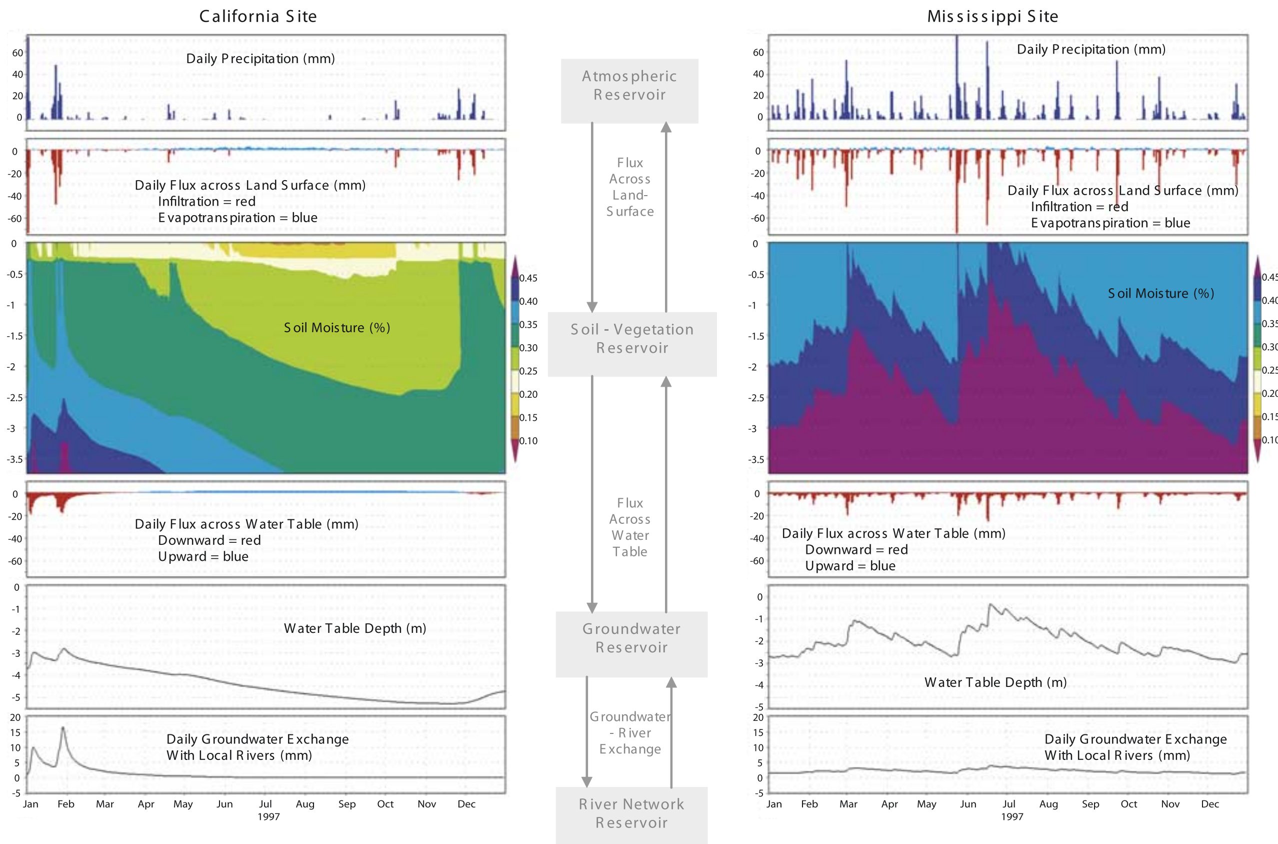

Figure 14. Linked evolution of soil moisture and water table through two-way fluxes among the reservoirs, at two model cells.

209 mm, and lateral groundwater gain is 138 mm, about 61% of the evaporative loss. The source of this lateral flow is likely the numerous losing streams at the foothills, which are themselves fed by snowmelt in the high mountains. At the Mississippi site, the primary control of the water budget is the vertical fluxes. Each precipitation event induces an infiltration event, which fills the soil pores and recharges the water table, which in turn adds water to the local rivers. Each interstorm period induces an evaporation flux, but it is relatively small and short-lived and only reduces the downward water table recharge without ever reversing the direction. At this site, the water table acts as a steady sink and a conveyer belt to deliver the atmospheric surplus to the rivers, and the resulting river flow is steady with little seasonal fluctuation. Together, the time series in Figure 14 illustrate how the precipitation forcing is filtered through the sequence of storages and fluxes on land in two contrasting hydrologic settings. Although both have a shallow water table, in each case it results from different hydrologic pathways and hence performs different functions in sustaining the land-atmosphere fluxes. In both cases, however, the water table plays a major role in determining how rainfall is partitioned between these pathways and reservoirs.

5. Summary

[40] In this second of two companion papers, we discussed the formulation and implementation of groundwater processes into RAMS by linking the groundwater and the rivers-lakes reservoir with its land surface scheme LEAF2, forming a new scheme LEAF2-Hydro.

[41] Before testing the impact of the new scheme on simulated soil moisture, we validated it with respect to streamflow and soil moisture observations. First, we tested the groundwater-surface water linkage separately by carrying out a 10-year simulation (1987–1996) driven by observationally based, daily forcing at the land surface. The simulated streamflow agrees well with observations at five locations in the Mississippi drainage.

[42] Next, we validated the linkage between the soil-vegetation reservoir and the groundwater-river system with a 1-year simulation (1997). LEAF2-Hydro captures the observed seasonal variations in evapotranspiration and stream flow. In addition, we compared with soil moisture observations from Illinois (humid) and Oklahoma (semiarid). Biases are due to mismatches between the soil texture in our 12.5 km model grid cell and the actual soil texture at the instrumentation site, and to biases in the initial soil moisture profile provided to the simulation.

[43] To highlight the role of the water table in controlling soil moisture, we compare the results of our 1997 soil moisture simulation with that of another simulation, otherwise identical, but that uses the commonly adopted free-drain approach. We focus on the warm season. Spatially, we see that wherever the water table is reasonably shallow, the near-surface and root zone soil moisture is significantly higher in the full hydrology run compared to the free-drain run. This is because of the slow vertical drainage due to the

presence of the water table as the lower boundary of the soil, the upward capillary flux from the water table as a source for dry-period evapotranspiration, and, in certain mountain valleys, the presence of lateral groundwater convergence. Temporally, the slow changing nature of the water table acts to stabilize the temporal variations in the soil moisture, giving the latter stronger seasonal persistence compared to the free-drain run.

[44] Since soil moisture is a critical control on land-atmosphere fluxes, these findings may have important implications to understanding land-atmosphere feedbacks though boundary layer climate dynamics. In a subsequent report, we will examine the next link: the spatial-temporal behavior of soil moisture and the spatial-temporal structures of the boundary layer dynamics and thermal dynamics, and the resulting precipitation, and further land-atmosphere feedbacks.

[45] **Acknowledgments.** This research is supported by the following grants: NSF EAR-0340780, NSF ATM-0450334, NOAA NA16GP1618, and New Jersey Department of Environmental Protection SR03-073. The first author is supported by the Ramón y Cajal program of the Spanish Ministry of Education and Science. In this work, we made use of VIC retrospective hydrologic simulations [*Maurer et al.*, 2002; *Nijssen et al.*, 2001], and we gratefully acknowledge their efforts in producing such a valuable data set for the community. Finally, we thank the reviewers and Editor for their constructive comments which helped to improve the manuscript significantly.

References

Arora, V. K., and G. J. Boer (1999), A variable velocity flow routing algorithm for GCMs, *J. Geophys. Res.*, *104*(D24), 30,965–30,979.

Basara, J. B., and T. M. Crawford (2000), Improved installation procedures for deep layer soil moisture measurements, *J. Atmos. Oceanic Technol.*, *17*, 879–884.

Beven, K. J., and M. J. Kirkby (1979), A physically-based variable contributing area model of basin Hydrology, *Hydrol. Sci. Bull.*, *24*, 43–69.

Chen, J., and P. Kumar (2001), Topographic influence on the seasonal and interannual variation of water and energy balance of basins in North America, *J. Clim.*, *14*(9), 1989–2014.

Clapp, R. B., and G. M. Hornberger (1978), Empirical equations for some soil hydraulic properties, *Water Resour. Res.*, *14*(4), 601–604.

Decharne, A., R. D. Koster, M. J. Suarez, M. Stieglitz, and P. Kumar (2000), A catchment-based approach to modeling land surface processes in a general circulation model: 2. Parameter estimation and model demonstration, *J. Geophys. Res.*, *105*(D20), 24,823–24,838.

de Vries, J. J. (1994), Dynamics of the interface between streams and groundwater systems in lowland areas, with reference to stream net evolution, *J. Hydrol.*, *155*, 39–56.

de Vries, J. J. (1995), Seasonal expansion and contraction of stream networks in shallow groundwater system, *J. Hydrol.*, *170*, 15–26.

Dunne, T., and R. D. Black (1970a), An experimental investigation of runoff production in permeable soils, *Water Resour. Res.*, *6*, 478–490.

Dunne, T., and R. D. Black (1970b), Partial area contributions to storm runoff in a small New England watershed, *Water Resour. Res.*, *6*, 1296–1311.

Eltahir, E., and P. J.-F. Yeh (1999), On the asymmetric response of aquifer water level to floods and droughts in Illinois, *Water Resour. Res.*, *35*, 1199–1217.

Fan, Y., G. Miguez-Macho, C. P. Weaver, R. Walko, and A. Robock (2007), Incorporating water table dynamics in climate modeling: 1. Water table observations and equilibrium water table simulations, *J. Geophys. Res.*, *112*, D10125, doi:10.1029/2006JD008111.

Gedney, N., and P. M. Cox (2003), The sensitivity of global climate model simulations to the representation of soil moisture heterogeneity, *J. Hydrometeorol.*, *4*, 1265–1275.

Gusev, Y. M., and O. N. Nasonova (2002), The simulation of heat and water exchange at the land-atmosphere interface for boreal grassland by the land-surface model SWAP, *Hydrol. Processes*, *16*, 1893–1919.

Gutowski, W. J., Jr., C. J. Vörösmarty, M. Person, Z. Ötles, B. Fekete, and J. York (2002), A Coupled Land-Atmosphere Simulation Program (CLASP): Calibration and validation, *J. Geophys. Res.*, *107*(D16), 4283, doi:10.1029/2001JD000392.

Habets, F., P. Etchevers, C. Golaz, E. Leblois, E. Ledoux, E. Martin, J. Noilhan, and C. Ottlé (1999), Simulation of the water budget and the river flows of the Rhone basin, *J. Geophys. Res.*, *104*(D24), 31,145–31,172.

Harbaugh, A. W., E. R. Banta, M. C. Hill, and M. G. McDonald (2000), Modflow-2000, the U.S. Geological Survey modular groundwater model—User guide to modularization concepts and the groundwater flow process, *U.S. Geol. Surv. Open File Rep., 00-92*.

Hewlett, J. D., and A. R. Hibbert (1963), Moisture and energy conditions with a sloping soil mass during drainage, *J. Geophys. Res.*, *68*, 1081–1087.

Hollinger, S. E., and S. A. Isard (1994), A soil moisture climatology of Illinois, *J. Clim.*, *7*, 822–833.

Kalnay, E. M., et al. (1996), The NCEP/NCAR 40-year reanalysis project, *Bull. Am. Meteorol. Soc.*, *77*, 437–472.

Koster, R. D., M. J. Suarez, A. Ducharne, M. Stieglitz, and P. Kumar (2000), A catchment-based approach to modeling land surface processes in a general circulation model: 1. Model structure, *J. Geophys. Res.*, *105*(D20), 24,809–24,822.

Liang, X., Z. Xie, and M. Huang (2003), A new parameterization for surface and groundwater interactions and its impact on water budgets with the variable infiltration capacity (VIC) land surface model, *J. Geophys. Res.*, *108*(D16), 8613, doi:10.1029/2002JD003090.

Lucas-Picher, P., V. K. Arora, D. Cayan, and R. Laprise (2003), Implementation of a large-scale variable velocity river flow routing algorithm in the Canadian Regional Climate Model (CRCM), *Atmos. Ocean*, *41*, 139–153.

Marani, M., E. Eltahir, and A. Rinaldo (2001), Geomorphic controls on regional base flow, *Water Resour. Res.*, *37*, 2619–2630.

Maurer, E. P., A. W. Wood, J. C. Adam, D. P. Lettenmaier, and B. Nijssen (2002), A long-term hydrologically-based data set of land surface fluxes and states for the conterminous United States, *J. Clim.*, *15*, 3237–3251.

Maxwell, R. M., and N. L. Miller (2005), Development of a coupled land surface and groundwater model, *J. Hydrometeorol.*, *6*, 233–247.

Nijssen, B., S. Reiner, and D. P. Lettenmaier (2001), Global retrospective estimation of soil moisture using the Variable Infiltration Capacity land surface model, 1980–93, *J. Clim.*, *14*, 1790–1808.

Niu, G. Y., and Z. L. Yang (2003), The versatile integrator of surface atmospheric processes—Part 2: evaluation of three topography-based runoff schemes, *Global Planet. Change*, *38*(1)–(2), 191–208.

Roads, J., and A. Betts (2000), NECP/NCAR and ECMWF eeanalysis surface water and energy budgets for the Mississippi River Basin, *J. Hydrometeorol.*, *1*, 88–94.

Robock, A., K. Y. Vinnikov, G. Srinivasan, J. K. Entin, S. E. Hollinger, N. A. Speranskaya, S. Liu, and A. Namkhai (2000), The Global Soil Moisture Data Bank, *Bull. Am. Meteorol. Soc.*, *81*, 1281–1299.

Robock, A., et al. (2003), Evaluation of the North American Land Data Assimilation System over the Southern Great Plains during the warm season, *J. Geophys. Res.*, *108*(D22), 8846, doi:10.1029/2002JD003245.

Seuffert, G., P. Gross, C. Simmer, and E. F. Wood (2002), The influence of hydrologic modeling on the predicted local weather: Two-way coupling of a mesoscale weather prediction model and a land surface hydrologic model, *J. Hydrometeorol.*, *3*, 505–523.

Walko, R. L., et al. (2000), Coupled atmosphere-biophysics-hydrology models for environmental modeling, *J. Appl. Meteorol.*, *39*, 931–944.

Weeks, J. B., E. D. Gutentag, F. J. Heimes, and R. R Luckey (1988), Summary of the High Plains regional aquifer-system analysis in parts of Colorado, Kansas, Nebraska, New Mexico, Oklahoma, South Dakota, Texas, and Wyoming, *U.S. Geol. Surv. Prof. Pap., 1400-A*.

Yang, Z. L., and G. Y. Niu (2003), The versatile integrator of surface and atmosphere processes (VISA)—Part 1: Model description, *Global Planet. Change*, *38*, 175–189.

Yeh, P. J.-F., and E. A. B. Eltahir (2005a), Representation of water table dynamics in a land surface scheme, part I: Model development, *J. Clim.*, *18*, 1861–1880.

Yeh, P. J.-F., and E. A. B. Eltahir (2005b), Representation of water table dynamics in a land surface scheme, part II: Subgrid variabiliy, *J. Clim.*, *18*, 1881–1901.

York, J. P., M. Person, W. J. Gutowski, and T. C. Winter (2002), Putting aquifers into atmospheric simulation models: An example from Mill Creek Watershed, northeastern Kansas, *Adv. Water Res.*, *25*(2), 221–238.

Y. Fan, Department of Geological Sciences, Rutgers University, Piscataway, NJ 08854-8066, USA. (yingfan@rci.rutgers.edu)

G. Miguez-Macho, Nonlinear Physics Group, Universidade de Santiago de Compostela, E-15706 Santiago de Compostela, Spain. (gonzalo@fmares.usc.es)

A. Robock and C. P. Weaver, Department of Environmental Sciences, Rutgers University, New Brunswick, NJ 08901-8551, USA. (robock@envsci.rutgers.edu; weaver@cep.rutgers.edu)

R. Walko, Department of Civil Engineering, Duke University, Durham, NC 27708, USA. (robert.walko@duke.edu)